
STRENGTH
AND PLASTICITY

Microstructure Evolution and Mechanical Properties of AISI 316H Austenitic Stainless Steel Processed by Warm Multi-Pass ECAP

K. Hajizadeh^{a, *} and K. J. Kurzydowski^b

^a Department of Mining and Metallurgical Engineering, Urmia University of Technology, Urmia, Iran

^b Faculty of Mechanical Engineering, Bialystok University of Technology, Bialystok, Poland

*e-mail: kaveh.hajizadeh@uut.ac.ir

Received October 2, 2020; revised January 20, 2021; accepted June 16, 2021

Abstract—AISI 316H austenitic stainless steel was subjected to equal channel angular pressing (ECAP) at 350°C up to eight passes and the resultant mechanical properties were compared with those obtained after cold rolling as representative for a cold worked state. A high density of thin parallel slip bands was observed inside coarse grains at the beginning of ECAP. Intense micro shear banding took place when pressing was continued by adding more passes. While no martensitic transformation was detected in the microstructure deformation twinning identified to occur at late passes of ECAP. The final microstructure after 8 passes is characterized by a tri-modal grain size distribution with equiaxed ultrafine grains of 176 nm and regions with larger grains of 217–1376 nm surrounded by shear bands containing nano-crystalline grains. Nano twins, 8 nm on average wide, were observed inside the nanocrystalline austenite grains. The observed microstructural features were explained by the stacking fault energy and temperature range for martensitic transformation of the studied material. In terms of mechanical properties, the processed material displayed a combination of very high yield strength exceeding 1550 MPa (close to four times the initial value) and good ductility with deformation $\epsilon_f = 11.6\%$ at failure.

Keywords: 316H stainless steel, equal channel angular pressing (ECAP), nanocrystalline structure, mechanical properties, grain size effect

DOI: 10.1134/S0031918X21300013

INTRODUCTION

AISI 316H is a molybdenum-bearing grade austenitic stainless steel with extreme resistance to pitting and crevice corrosion in high chloride environments [1]. It is widely utilized in the manufacturing of chemical processing and storage equipment. The major disadvantage of this steel is a low yield strength (YS) [2]. Cold working by, for example rolling, is an obvious method of increasing its resistance to plastic deformation, however, it causes a sharp decrease in ductility [3]. In this context strengthening by the grain size refining is more efficient, which preserves or even increases the ductility of FCC metals [4, 5].

Severe plastic deformation (SPD) has been established over the last years as a practical approach to grain size refinement [3, 5, 6]. Different SPD methods such as equal channel angular pressing (ECAP) [2, 7], High-pressure torsion (HPT) [8], and Hydrostatic extrusion [9] have been successfully applied on austenitic stainless steels. As a result, a nanocrystalline structure ($d < 100$ nm) were commonly obtained and led to a significant enhancement of the yield and ultimate strengths [7–9].

Dislocation slip, twinning, and stress-induced martensitic transformation are typical deformation mechanisms in austenitic stainless steels [2]. One of the factors that plays a key role in the occurrence of each of these mechanisms during deformation is the stacking fault energy (SFE) of the material [2]. SFE is a function of the chemical composition and in this respect carbon is a very effective element [7]. Hence, different microstructural evolutions in type 316H which is a higher carbon variant of 316 than in 316L is expected to occur during SPD processing. This in turn can affect the degree of refinement of the initial microstructure and the resultant mechanical properties of the processed material. Despite much activity in ECAP processing of 316 stainless steel, the literature review shows that in most of earlier researches type 316L has been studied. The present work is an attempt to investigate the deformed microstructure and mechanical properties of type 316H stainless steel during ECAP processing. In this regard, Light (LM) and scanning transmission electron microscopy (STEM) were used for microstructure observations. Tensile and hardness tests were carried out to evaluate

the effect of ECAP processing on the mechanical properties of the steel.

EXPERIMENTAL PROCEDURE

The material used in this investigation was a hot rolled commercial AISI 316H type austenitic stainless steel. The bulk nominal composition was 16.5% Cr, 13.8% Ni, 2.8% Mo, 0.079% C, 0.10% N, 1.68% Mn, 0.42% Si, and Fe for the balance. First, the material was annealed at 1150°C for one hour, and then, water quenched. The samples for ECAP processing 70 mm in length with a diameter of 14.5 mm were machined from the annealed material. These samples were subjected to ECAP in a die with channels intersecting at an inner angle of $\Phi = 105^\circ$ and outer angle of $\Psi \approx 20^\circ$, which yields an effective strain of about 0.8 per pass [10]. ECAP was performed for up to 8 passes at 350°C at a constant ram speed of 1 mm s⁻¹ using route B_C whereby the billet was rotated by 90° counterclockwise between successive passes. The microstructures of the as-pressed samples were observed by both light microscope (LM) and scanning transmission electron microscope (Hitachi HD 2700, operating at 200 kV).

Specimens for STEM observations were cut from middle sections of the pressed billets parallel to the pressing direction. Thin foils for STEM were first mechanically ground to about 40 μm and finally electropolished in a Tenupol 5 double jet polishing unit in a solution of 10 vol % perchloric acid and ethanol at room temperature.

To evaluate the mechanical behavior of the processed material, microhardness and tensile tests were carried out. Vickers microhardness (H_v) was carried out using a microhardness tester Future-Tech FM-700 on the plane parallel to the longitudinal axis with a load of 200 g with a holding time of 15 s. Tensile test specimens of 2 × 3 × 12 mm were cut along the longitudinal axis of billets according to JIS Z2201 standard. All tensile tests were conducted at room temperature using an MTS 810 servo-hydraulic testing machine operating at an initial strain rate of 5 × 10⁻³ s⁻¹. Experiments were repeated on three companion specimens to check repeatability.

X-ray diffraction (XRD) patterns were recorded on a Bruker AXS D8-ADVANCE diffractometer using Cu K α radiation of 0.15406 nm wavelength, 40 kV, and 50 mA. Patterns were collected over the 2 θ range of 40°–100° with a step size of 0.01° per step and a dwell time of 1 s per increment.

To gain a better understanding of difference between SPD processing by ECAP and cold worked state, cold rolling (CR) was applied at room temperature on two samples of starting material after annealing treatment. CR samples had rectangular sections with dimensions of 12 mm × 12 mm × 70 mm. Thickness reductions of 50 and 90% were applied on samples without any intermediate annealing.

RESULTS

Figure 1 shows the light microscopy images representing the microstructure of AISI 316H stainless steel before and after 1 to 8 passes of ECAP. The initial microstructure (Fig. 1a) consists of equiaxed grains with an average intercept length of ~57 μm. Besides, inside some grains, annealing twins with orientations varying from grain to grain are seen. Inclusions with less than a few micrometres in size are sometimes found. After a single pass of ECAP, the initial equiaxed grains became severely elongated and subdivided into fragments. A high density of thin parallel slip bands of 1.6 μm average width can be detected in the interior of some grains. An example of these bands is shown in the magnified image, Fig. 1c. Slip steps (indicated by arrows) are clearly seen at the end of the bands demonstrating the fact that they are slip bands and formed as a result of a slip, not twinning. After two passes, a partly non-uniform microstructure was observed. Regions with highly elongated grains (surrounded by an ellipse in Fig. 1d) broken up into fragments of a few micrometer sizes (e.g. indicated by arrows), along with initial coarse grains which are slightly elongated (denoted by letter A in Fig. 1d) are simultaneously visible in the structure. Refined regions are probably those containing grains favorably oriented to slip, which have deformed enough whereby relatively fine fragments have been formed there. Another feature of the microstructure after two passes is the formation of localized deformation region in the form of shear bands within some initial coarse grains. An example of such shear bands is marked with a number of short black arrows in Fig. 1d. Further pressing to 3 passes results in the more homogenous microstructure. All of the grains cut by numerous fine bands. The intersection of slip bands (like those surrounded by two circles in Fig. 1e) is frequently occurred and led to the fragmentation of lamellas established in early passes. Bands intersection is caused by the activation of different slip systems in consecutive passes, because rotations of sample about its longitudinal axis change the shearing plane [8]. After six passes, the microstructure has experienced significant changes: First, initial grain boundaries are no longer recognizable. Second, widespread shear banding has occurred throughout the microstructure (some of them indicated by arrows in Fig. 1f). Third, outside the shear bands, the microstructure intensely refined so that many equiaxed ultra-fine grains or very short/thin bands have been formed in most regions. (An example of such regions is illustrated by a circle in Fig. 1g which is a higher magnification image of the six-pass sample.) Figure 1g reveals two characteristic features in the shear band region: (1) elongated grain structure; generally, less than 1 μm in width, extended in the shear direction (like those surrounded by two ellipses in Fig. 1g) and (2) submicron size equiaxed grains (illustrated by a rectangle). Finally, Fig. 1h shows the microstructure after eight passes of ECAP processing which is very

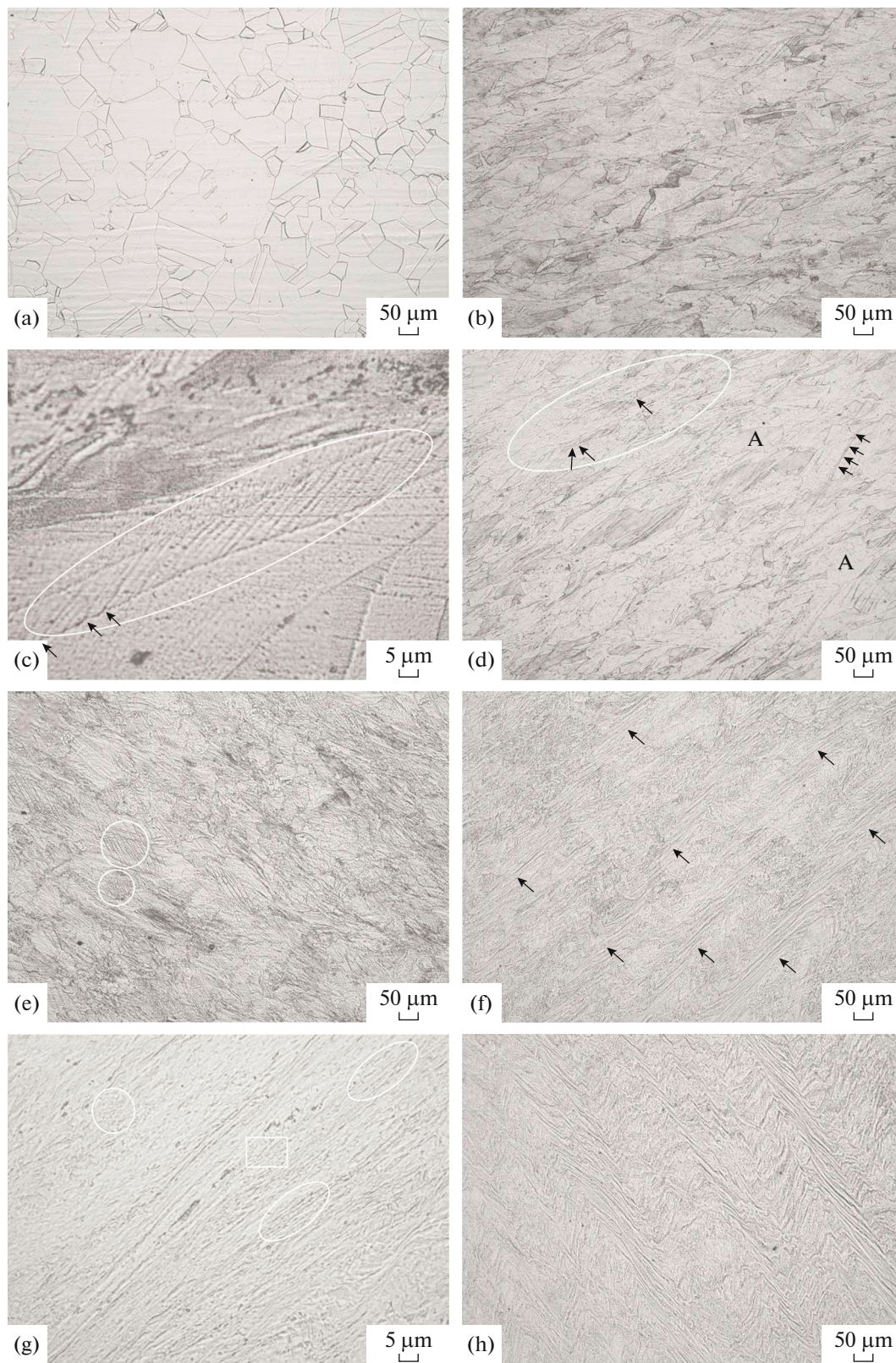


Fig. 1. Light microscopy micrographs showing the microstructure of AISI 316H stainless steel: (a) before ECAP, and after repetitive ECAP: (b, c) 1 pass, (d) 2 passes, (e) 3 passes, (f, g) 6 passes, and (h) 8 passes.

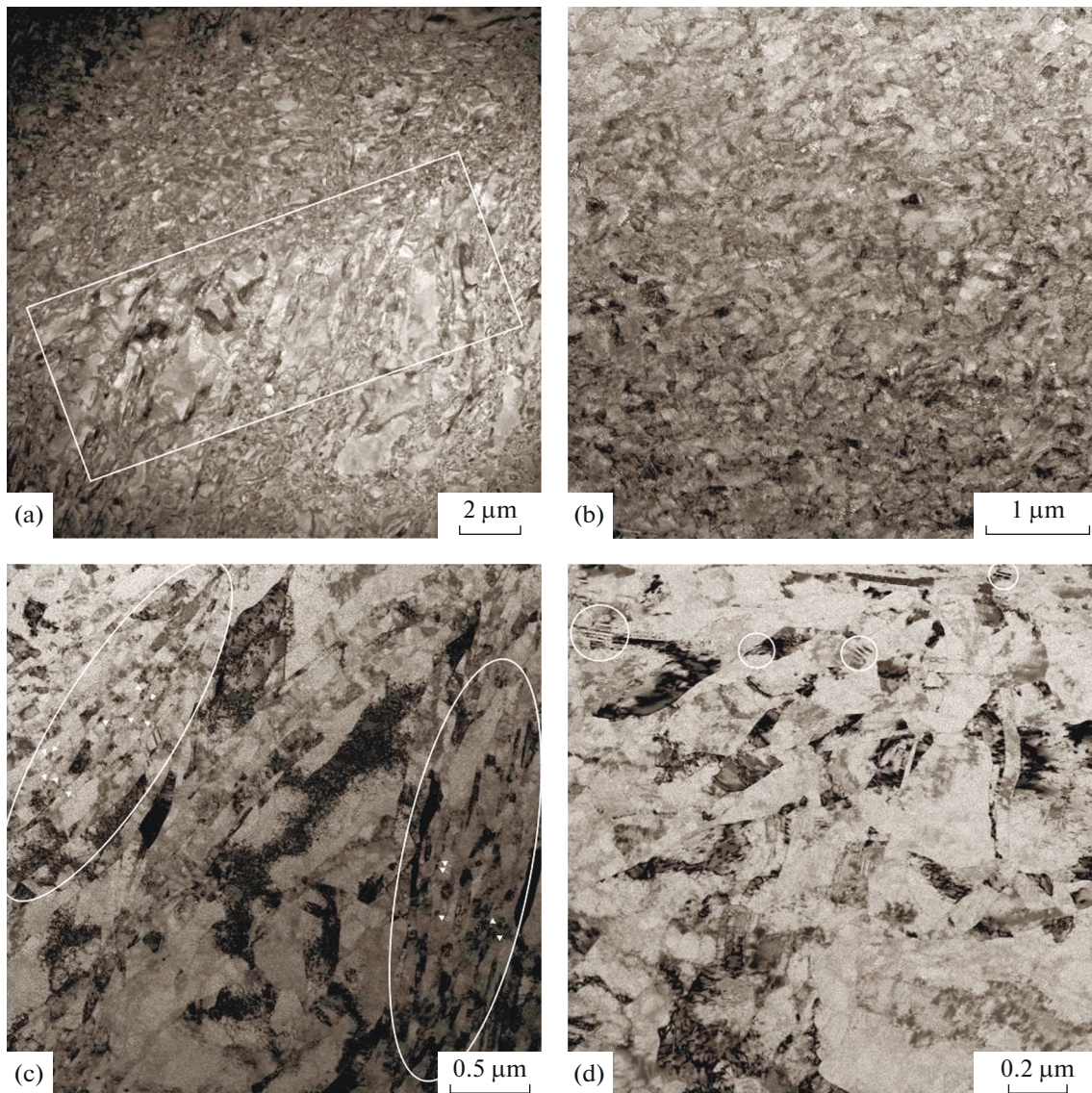


Fig. 2. Microstructures of AISI 316H stainless steel by STEM after ECAP through 8 passes at 350°C taken from the longitudinal section of a processed bar: (a, b) low and (c, d) high magnifications.

similar to that of pass 6. This microstructure was examined by STEM, and its details are presented below in Fig. 2.

As is expected, during straining to a level of equivalent strain of 6.4, the initial coarse-grained structure has experienced an apparent refinement from tens of microns down to ultrafine/nanocrystalline range. The microstructure exhibits a tri-modal character (Fig. 2a) consisting of regions mostly with equiaxed ultrafine grains of 176 nm average size (an example of them is shown in Fig. 2b) and regions with larger grains of 217–1376 nm surrounded by and/or included in bands of extremely fine elongated grains (for example, the areas enclosed by a rectangle in Fig. 2a). A typical higher magnification image from these regions is shown in Fig. 2c. Relatively large grains with submi-

cometer size are observed in the middle part of the image surrounded by two sets each containing a large number of short/thin bands. The regions containing these thin lamellae (surrounded by two ellipses in Fig. 2c), in fact, are the same shear localization regions (shear bands) previously appeared in metallographic images. The microstructure within the shear bands is mainly composed of elongated grains with an average length of 228 nm and the average width of 66 nm. However, extremely fine equiaxed grains generally less than 50 nm in size could also be frequently found (e.g. the grains indicated by short white arrows in Fig. 2c).

Another type of grain structure can be seen in some areas. Ultrafine grains, though small in number, are found in the structure within which there are several

flat interfaces parallel to each other (circles in Fig. 2d mark some of such grains). The average width of these ultra thin bands measured to be just 8 nm. Later, it will be discussed that the martensitic phase has very little chance to form in the studied steel, so these ultra-narrow bands are most likely deformation twins. Formation of nano twins is a common feature observed during severe plastic deformation of low stacking fault energy materials such as AISI 316 stainless steel [2, 8].

Figure 3 shows the engineering stress-strain curves of AISI 316H stainless steel obtained by room temperature tensile tests for the starting material along with the samples subjected to ECAP for different number of passes. In addition, the curves for the 50 and 90% cold rolled samples as representatives of the cold worked state are also included. The tensile properties extracted from the stress-strain curves together with the microhardness values of samples are given in Table 1. It is seen that the microhardness increased from 148 HV, related to as-annealed sample, to 309 HV after the single pass of ECAP and rises to 350 HV in the second pass. Thereafter, it enhances slightly to a maximum value of 426 HV after a total of eight passes. It can be seen from Fig. 3 and Table 1 that in general, processing eight passes by ECAP led to a remarkable improvement of yield strength by about four times from 407 to 1584 MPa and ultimate tensile strength by more than twice from 753 to 1670 MPa. This significant strengthening is accompanied with obvious loss in ductility wherein elongation to failure (ϵ_f) decreases from 51% in the starting material to ~12% after eight passes of ECAP. It is apparent also that, cold rolling has greatly enhanced the strength and hardness of AISI 316H stainless steel. It is seen that UTS of the sample subjected to preliminary 50% thickness reduction reach 1160 MPa, the value is comparable with that of three passes ECAP-ed sample, and then it approaches to ~1700 MPa after 90% thickness reduction which is more than the UTS corresponding to the sample deformed by ECAP for eight passes. At the same time, cold rolled material shows poor ductility of $\epsilon_f = 10.7$ and 6.4% respectively after 50 and 90% thickness reduction.

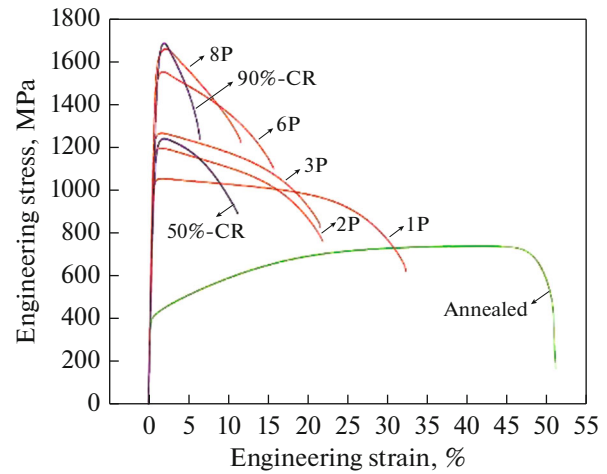


Fig. 3. Room temperature tensile engineering stress-strain curves of AISI 316H stainless steel obtained after different processing condition: annealed material (green curve), after ECAP for different number of passes (red curves) and, after 50 and 90% thickness reduction by cold rolling (blue curves).

DISCUSSION

Austenitic stainless steels are deformed by various deformation mechanisms. Dislocation slip, twinning, stress-induced martensitic transformation are typical phenomena in these steels that the occurrence of each of them depends mainly on the amount of stacking fault energy (SFE) of the material, and on the processing conditions such as deformation temperature and speed [2]. Depending on the material chemical composition the SFE of Austenitic stainless steels varies from 9.2 to 80.7 mJ/m² [7]. In the literature, the sequence of deformation mechanisms of austenitic steels by decreasing stacking fault energy is reported as follows [11]: at the SFE < 20 mJ/m² the martensitic transformation ($\gamma \rightarrow \alpha_{bcc}$ or $\gamma \rightarrow \epsilon_{hcp}$) is the dominant mechanisms. At stacking fault energies roughly in the range of 20 < SFE < 45 mJ/m² twinning occurs. In the range of SFE value above 45 mJ/m², plastic deformation is controlled by dislocation slip. SFE of austenitic

Table 1. Tensile properties of AISI 316H steel after processing in the different deformation conditions

Processing conditions	YS, MPa	UTS, MPa	ϵ_f , %	ϵ_u , %	Microhardness, HV
Annealed	407	753	51	40.9	148
ECAP- 1P	1036	1066	32.2	1.68	309
ECAP- 2P	1173	1208	21.9	1.72	350
ECAP- 3P	1240	1278	21.6	1.64	367
ECAP- 6P	1486	1564	15.7	1.86	405
ECAP- 8P	1584	1670	11.6	2.15	426
50% Cr	1160	1253	10.7	1.92	348
90% Cr	1557	1697	6.4	1.94	415

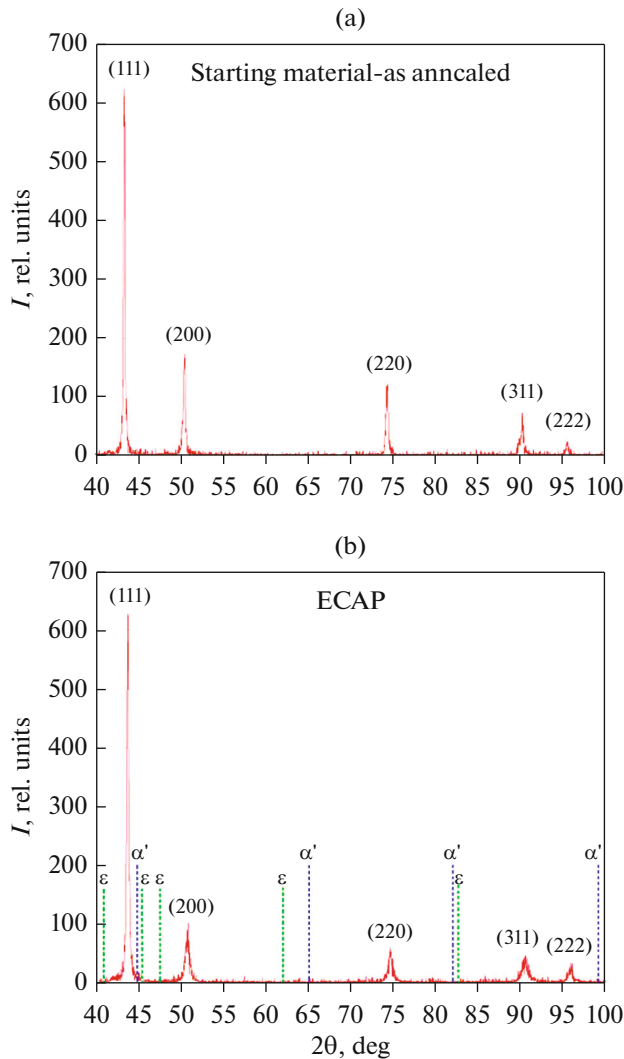


Fig. 4. XRD patterns of AISI 316H stainless steel related to: (a) initial coarse-grained material after annealing, (b) after 8 passes of ECAP at 350°C. Dash lines in (b) indicate the positions where the peaks associated with α' and ϵ martensitic phases appear if they exist.

steels can be estimated according to their chemical composition by the following experimental equation [7]:

$$\begin{aligned} \text{SFE} \left(\text{mJ/m}^2 \right) \\ = 25.7 - 2.0 \times \% \text{Ni} + 410.0 \times \% \text{C} - 0.9 \times \% \text{Cr} \quad (1) \\ - 77.0 \times \% \text{N} - 13.0 \times \% \text{Si} - 1.2 \times \% \text{Mn}. \end{aligned}$$

Where weight percentages are used.

For the nominal chemistry of the steel used in the present study this formula gives the following estimate of $\text{SFE} = 55.4 \text{ mJ/m}^2$.

With this value of SFE the literature data [12] show that the dominant deformation mechanism during ECAP processing is expected to be dislocation slip, in agreement with the results of microstructural observa-

tions. Similar formula can be used to estimate the temperatures range for martensitic transformation: M_s (martensitic transformation start temperature), and M_{d30} (the lowest temperature at which 50% α' martensite is formed during deformation at 30% true strain).

The magnitude of these temperatures obtained as $M_s = -555^\circ\text{C}$, $M_{d30} = -96^\circ\text{C}$ using the formula presented in [7]. Accordingly, martensitic transformation is unlikely to take place during processing at 350°C in the case of the steel used in this study because of relatively high amount of carbon and nitrogen in the chemical composition of the steel, which are known as strong austenite stabilizers. This is also supported by the results of XRD analysis shown in Fig. 4 where no diffraction peaks belonging to α' or ϵ martensite are observed.

Byun et al. [12] have shown that formation of twins in AISI 316 and AISI 316LN stainless steels depends heavily on the magnitude of external applied stress. They proposed an expression to estimate a critical stress level beyond which twin nucleation occurs:

$$\sigma_T = \frac{1}{\text{SF}} \frac{2\gamma_{\text{SFE}}}{b}, \quad (2)$$

Where σ_T is the uniaxial critical twinning stress, γ_{SFE} denotes the material's stacking fault energy, SF is the average Schmidt factor, and b is the abs.value of Burgers vector. By substituting 145 nm for b and the calculated value of 55.4 mJ/m² for γ_{SFE} and supposing a Schmidt factor of 0.5 in accordance with Moallemi [13] and Talonen and Hanninen's studies [14], the critical twinning stress is obtained as 1528 MPa, which is well above the amount reported by Byun et al. (i.e., $\sigma_T = 600 \text{ MPa}$ for room temperature). This big difference can be arising from first: the difference in γ_{SFE} of the present steel with that used in their study and second, from the difference in deformation temperature used in two studies. It is expected that twinning occurs more difficult with increasing deformation temperature, because twinning stress increases with increasing temperature.

Figure 5 shows the pressing load-displacement curves recorded during ECAP processing of the present AISI 316H steel at 350°C up to eight passes. It can be seen that the steady state load required for single pass of ECAP processing was about 139 kN and increased gradually with further passes and eventually reached to about 252 kN during eight pass. Dividing the recorded loads by cross section area of the billet, the maximum normal stresses applied to the billets are obtained 844, 945, 1068, 1312, and 1530 MPa respectively for 1, 2, 3, 6, and 8 passes. By comparing these stress values with critical twinning stress level calculated for studied material by equation (2) (i.e.: $\sigma_T = 1528 \text{ MPa}$) one can notice that twinning is likely to occur in late passes of ECAP where experimental applied normal stress exceeded critical calculated value like what is seen for the eight pass. This suggests

that the ultra-thin parallel bands formed inside some nanocrystalline grains (circles in Fig. 2d) are most likely to be twin bands.

A comparison between the obtained strength and hardness values after ECAP with those measured for the cold rolled samples shows that cold working is also as effective as ECAP or even more effective than it in strengthening of AISI 316H stainless steel. The distinctive aspect of ECAP with cold rolling is that, because the sample maintains its same cross-sectional area during ECAP, the use of repetitive pressing is feasible to provide an opportunity of imposing high levels of plastic strain into the material. This allows the low angle boundaries formed at low strains during initial passes to evolve into high angle ones through the absorption of more lattice dislocations [10].

In contrast, such evolution cannot occur in conventional deformation processes such as cold rolling because of the inherent limitation in imposing more strain by them that comes from a reduction occurring in sample thickness. As a result, in spite of ECAP processed materials which contain arrays of ultrafine grains surrounded by mainly high angle grain boundaries [15], the cold-rolled microstructures in FCC metals generally consist of cell structures and subgrains which are separated by low-angle boundaries [3, 10]. Subgrain boundaries are not strong barriers against movement of dislocations and are penetrable. So at first glance, it may be expected that the cold rolled structure will show less strength than ECAP-ed one. However, it should be noted that while rolling was performed at room temperature, ECAP was conducted at warm deformation region ($T = 350^{\circ}\text{C}$). It is quite clear that an increase in deformation temperature reduces the dislocation density inside grains, because it accelerates thermally activated deformation mechanisms such as dislocation climb, cross slip, and etc. Therefore, the high strength of cold rolled material can be attributed mainly to its much higher dislocation density compared to ECAP-ed material. Additionally, it is reasonable to consider that cold rolled structure receives more contribution from thin twins and their boundaries to be strengthened, because twinning occurs more easily at lower deformation temperatures. The main advantage of ECAP processed microstructure over cold worked state (cold rolled material here) is that in spite of its great strength, it still retains a reasonable ductility. We don't see such behavior in cold rolled material. For example, while the strength of 90% cold rolled sample and 8 pass ECAP-ed material are almost identical, ductility after ECAP is close to twice of that obtained after cold rolling ($\epsilon_{f(\text{ECAP})} = 11.6\%$ against $\epsilon_{f(\text{CR})} = 6.4\%$). The same trend in evolution of ductility was observed in Aluminium alloy 3004 [15] where ECAP resulted in ultimately to a higher retention of ductility than cold-rolling. This behavior was attributed to a higher percent-

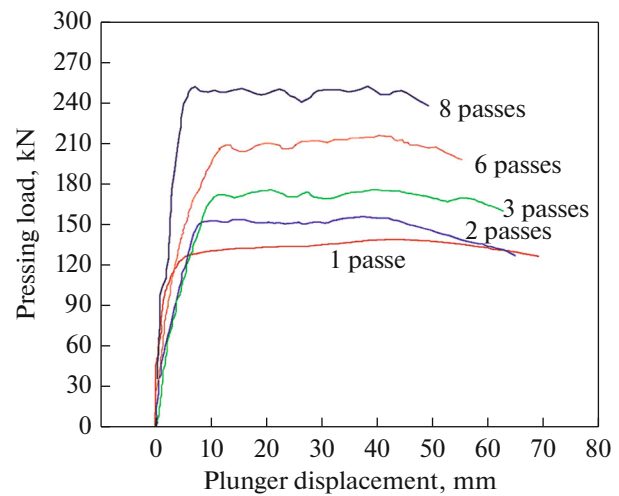


Fig. 5. Pressing load–plunger displacement curves recorded for AISI 316H stainless steel at 350°C during ECAP through different number of passes.

age of high-angle grain boundaries inside ECAP processed microstructure and consequently to an increased role of grain boundary sliding and grain rotations as mechanisms that accommodate plastic deformation and contribute to obtaining good ductility [10, 16].

CONCLUSIONS

Equal channel angular pressing (ECAP) was conducted on type 316H stainless steel up to 8 passes. The following conclusions can be drawn from the results:

(1) In general, ECAP for 8 passes results in an apparent refinement from $57\ \mu\text{m}$ down to ultrafine/nanocrystalline range. The refined microstructure shows a tri-modal character of grain size distribution consisting of regions mostly with equiaxed ultrafine grains of $176\ \text{nm}$ and regions with larger grains of $217\text{--}1376\ \text{nm}$ surrounded by shear bands areas containing mainly nanocrystalline grains. Nano twins, $8\ \text{nm}$ average wide, are observed inside the nanocrystalline austenite grains after 8 passes.

(2) Formation of the UFG/NC structure in 316H stainless steel after 8 passes leads to a significant enhancement of:

- (a) Microhardness from 148 to 426 HV,
- (b) Yield strength from 407 to 1584 MPa, and
- (c) Ultimate tensile from 753 to 1670 MPa.

At the same time, a moderate ductility of 11.6% is maintained in the material.

(3) Despite similar strengthening capability, warm severe plastic deformation of AISI 316H steel by ECAP results in ultimately higher retention of ductility (nearly twice) than that of after cold rolling.

ACKNOWLEDGMENTS

The authors would like to thank Warsaw university of technology for their technical support, which made this research possible.

REFERENCES

1. S. Yu. Mushnikova, S. K. Kostin, V. V. Sagaradze, and N. V. Kataev, "Structure, properties, and resistance to stress-corrosion cracking of a nitrogen-containing austenitic steel strengthened by thermomechanical treatment," *Phys. Met. Metallogr.* **118**, 1155–1166 (2017).
2. G. G. Yapici, I. Karaman, Z.P. Luo, H.J. Maier, and Y.I. Chumlyakov, "Microstructural refinement and deformation twinning during severe plastic deformation of 316L stainless steel at high temperatures," *J. Mater. Res.* **19**, 2268–2278 (2004).
3. R. Z. Valiev, R. K. Islamgaliev, and I. V. Alexandrov, "Bulk nanostructured materials from severe plastic deformation," *Prog. Mater. Sci.* **45**, 103–189 (2000).
4. L. S. Vasilev and I.L. Lomaev, "On possible mechanisms of nanostructure evolution upon severe plastic deformation of metals and alloys," *Phys. Met. Metallogr.* **101**, 386–392 (2006).
5. I. G. Brodova, V. I. Zel'dovich, and I. V. Khomskaya, "Structure–Phase Transformations and Properties of Non-Ferrous Metals and Alloys under Extreme Conditions," *Phys. Met. Metallogr.* **121**, 631–663 (2020).
6. A. B. Nayzabekov and I. E. Volokitina, "Effect of the initial structural state of Cr–Mo high-temperature steel on mechanical properties after equal-channel angular pressing," *Phys. Met. Metallogr.* **120**, 177–183 (2019).
7. H. Ueno, K. Kakhata, Y. Kaneko, S. Hashimoto, and A. Vinogradov, "Nanostructurization assisted by twinning during equal channel angular pressing of metastable 316L stainless steel," *J. Mater. Sci.* **46**, 4276–4283 (2011).
8. S. Scheriau, Z. Zhang, S. Kleber, and R. Pippan, "Deformation mechanisms of a modified 316L austenitic steel subjected to high pressure torsion," *Mater. Sci. Eng., A* **528**, 2776–2786 (2011).
9. M. Pisarek, P. Kedzierzawski, M. Janik-Czachor, and K. J. Kurzydowski, "The effect of hydrostatic extrusion on resistance of 316 austenitic stainless steel to pit nucleation," *Electrochem. Commun.* **9**, 2463–2466 (2007).
10. R. Z. Valiev and T. G. Langdon, "Principles of equal-channel angular pressing as a processing tool for grain refinement," *Prog. Mater. Sci.* **51**, 881–981 (2006).
11. J. Lu, L. Hultman, E. Holmstrom, K. H. Antonsson, M. Grehk, W. Li, L. Vitos, and A. Golpayegani, "Stacking fault energies in austenitic stainless steels," *Acta Mater.* **111**, 39–46 (2016).
12. T. S. Byun, N. Hashimoto, and K. Farrell, "Temperature dependence of strain hardening and plastic instability behaviors in austenitic stainless steels," *Acta Mater.* **52**, 3889–3899 (2004).
13. M. Moallemi, A. Zarei-Hanzaki, and A. Mirzaei, "On the stacking fault energy evaluation and deformation mechanism of sanicro-28 super-austenitic stainless steel," *J. Mater. Eng. Perform.* **24**, 2335–2340 (2015).
14. J. Talonen and H. Hanninen, "Formation of shear bands and straininduced martensite during plastic deformation of metastable austenitic stainless steels," *Acta Mater.* **55**, 6108–6118 (2007).
15. S. N. Lezhneva, I. E. Volokitina, E. A. Panina, and A. V. Volokitina, "Evolution of the microstructure and mechanical properties of copper during the rolling–ECAP process," *Phys. Met. Metallogr.* **121**, 689–693 (2020).
16. Y. T. Zhu and T. G. Langdon, "The fundamentals of nanostructured materials processed by severe plastic deformation," *JOM* **56**, 58–63 (2004).
17. R. Z. Valiev, M. Yu. Murashkin, A. V. Ganeev, and N. A. Enikeev, "Superstrength of nanostructured metals and alloys produced by severe plastic deformation," *Phys. Met. Metallogr.* **113**, 1193–1201 (2012).